

Magnon driven chiral charge and spin pumping and electron-magnon scattering from time-dependent-quantum-transport/classical-micromagnetics framework

Abhin Suresh¹ and Branislav K. Nikolić^{1,2,*}

¹*Department of Physics and Astronomy, University of Delaware, Newark, DE 19716, USA*

²*Kavli Institute for Theoretical Physics, University of California, Santa Barbara, CA 93106-4030*

Using newly developed time-dependent-quantum-transport/classical-micromagnetics framework, we investigate interaction between conduction electrons and a single spin wave (SW) coherently excited within a metallic ferromagnetic nanowire. The classical micromagnetics describes SW as a collection of localized magnetic moments whose vectors of fixed length precess with harmonic variation in the phase of precession of adjacent moments around the local magnetization direction. Conversely, electrons interacting with SW are described quantum-mechanically using time-dependent nonequilibrium Green functions. When the nanowire hosting SW is attached to two normal metal (NM) leads, even in the absence of any external dc bias voltage between them the SW pumps *chiral* electronic charge and spin currents into the leads—they scale linearly with the frequency of the precession and their direction is tied to the direction of wave propagation. This is in contrast to standard pumping of *identical* spin currents in both directions, and *no* charge current, by the uniform precession mode. Upon applying dc bias voltage to inject spin-polarized charge current from the left NM lead, electrons interact with SW where we quantify outflowing charge and spin current into the right NM lead due to both scattering off time-dependent potential generated by the SW and superposition with the currents pumped by the SW itself. Finally, we use Lorentzian voltage pulse to excite the so-called “leviton” out of the Fermi sea, which carries two electron charges with no accompanying electron-hole pairs. The scattering of such soliton-like quasiparticle from the SW results in the change of its width and the corresponding charge and spin it carries.

The interaction of electrons with spin excitations—such as single-particle Stoner excitations or collective spin wave (SW) excitations—plays a fundamental role in equilibrium properties of bulk ferromagnetic metals (FM) since it can renormalize their electronic band structure [1–3]. As illustrated in Fig. 1, SW can be viewed semiclassically [4] as a disturbance in the local magnetic ordering in which localized magnetic moments start to precess around the easy axis with the phase of precession of adjacent moments varying harmonically in space over the wavelength λ . The quanta of energy of SW behave as a quasiparticle termed magnon carrying energy $\hbar\omega$ and spin \hbar . The frequency ω of the precession is commonly in GHz range of microwaves, but it can reach THz range in antiferromagnets [5]. The number of magnons measures deviation of a magnetic material from its perfect ordering in the ground state. The SWs can be excited in equilibrium as incoherent thermal fluctuations, which then reduce the total magnetization with increasing temperature. They can also be excited by external fields [6, 8–12] which leads to coherent propagation of SWs as a dispersive signal. The electron-magnon interaction can provide a glue for Copper pairs in magnon-mediated superconductivity [13–16]. It can also lead to the formation of composite particles, such as magnetic polaron, via hybridization of electronic and magnonic states [17–21].

Out of equilibrium, electron-magnon scattering is encountered in numerous phenomena in spintronics within magnetic layers or at their interfaces with layers of normal metals and insulators. For example, such processes

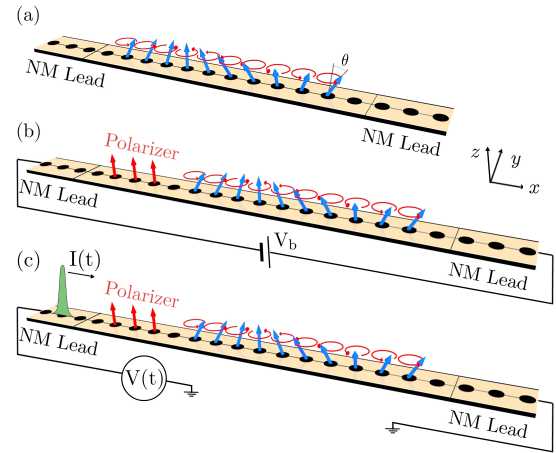


FIG. 1. Schematic view of two-terminal devices where FM wire, modeled as 1D chain of atoms [7], hosts SW comprised of ten localized magnetic moments precessing as classical vectors around the local easy axis direction with frequency ω and cone angle $\theta = 10^\circ$ [8], as well as with harmonic variation in the phase of precession of adjacent moments. The nanowire is attached to semi-infinite NM leads which terminate in macroscopic reservoirs. We consider three such setups: (a) no bias voltage is applied between the reservoirs; (b) small bias voltage V_b is applied to inject unpolarized charge current into the wire, which is then spin-polarized by three fixed spins (red arrows); and (c) Lorentzian voltage pulse [22, 23] is applied between the reservoirs to inject “leviton” current pulse $I_R(t)$ into the wire carrying charge $\int dt I_R(t) = 2e$.

can: increase resistivity of FM with temperature due to spin-flip scattering from thermal spin disorder [24, 25]; play an essential role in the laser-induced ultrafast de-

* bnikolic@udel.edu

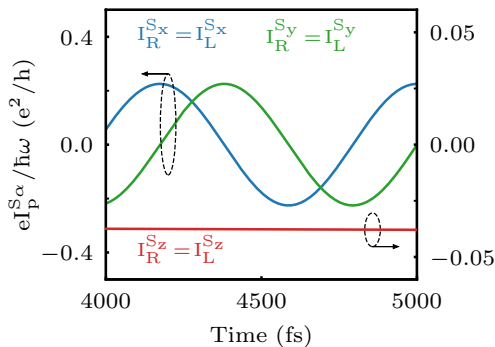


FIG. 2. Time-dependence of electronic spin currents $I_L^{S\alpha}(t) = I_R^{S\alpha}(t)$ pumped symmetrically into the left and right NM leads of setup in Fig. 1(a) whose localized magnetic moments precess as a uniform mode with $k = 0$ in Eq. (1). The Fermi energy is chosen as $E_F = -1.6$ eV and dc bias voltage is absent, $V_b = 0$.

magnetization [26]; generate nontrivial temperature and bias voltage dependence of tunneling magnetoresistance in magnetic tunnel junctions [27, 28]; open inelastic conducting channels [29]; contribute to spin-transfer [30, 31] and spin-orbit (SO) torque [32]; and convert magnonic spin currents into electronic spin current or vice versa at magnetic-insulator/normal-metal interfaces [12, 33, 34] (which includes processes in the spin Seebeck effect where magnonic spin currents are excited by temperature gradients [35]).

The nonequilibrium many-body perturbation theory [28, 34], formulated using Feynman diagrams for nonequilibrium Green functions [36], offers rigorous quantum-mechanical treatment of both electrons and magnons, once the original spin operators are mapped to the bosonic ones [37]. However, to ensure current conservation, one has to sum large classes of such diagrams [38] which can lead to errors due to missed vertex corrections [39]. Furthermore, due to small magnon bandwidth, small electron-magnon interaction constant J_{sd} in the realm of electrons can become strongly correlated regime for magnons due to large ratio $J_{sd}/\text{magnon-bandwidth}$. This can lead to quasibound states of magnons surrounded by electron-hole pairs [28], therefore suggesting that complicated higher order diagrams should be evaluated. This severely limits system size in two-terminal geometries of Fig. 1 or time scale over which electronic spin and charge currents, or magnonic spin current, can be computed. We recall that both electron and magnons have intrinsic angular momenta, so that translational flow of these particles or quasiparticles, respectively, leads to a flux of angular momentum.

On the other hand, experiments [6, 8–10] exciting dipole or exchange dominated SWs are commonly interpreted using classical micromagnetics simulations [4]. In such a picture, SW is described by trajectories of classical vectors $\mathbf{M}_i(t)$ of fixed (unit) length, pointing along the direction of localized magnetic moments, which precesses

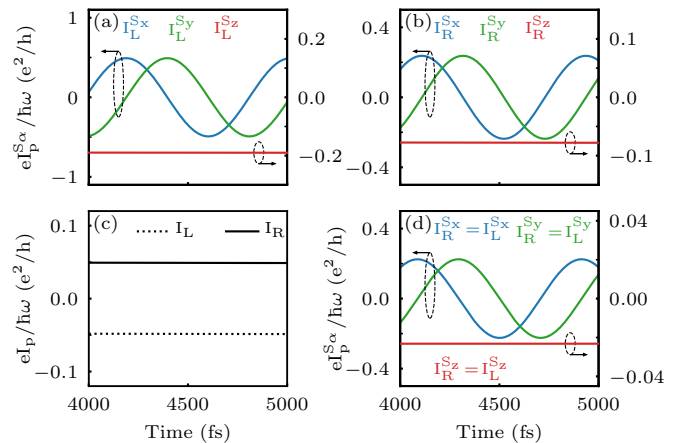


FIG. 3. Time-dependence of electronic spin currents pumped into the (a) left and (b) right NM leads of setup in Fig. 1(a) whose localized magnetic moments precess as coherent SW mode [46] with $k \neq 0$ in Eq. (1). (c) The SW with its nonuniform precessing magnetic moments also pumps steady charge currents $I_L = -I_R$ into the NM leads. Panel (d) shows pumping of only spin currents, symmetrically into both leads $I_L^{S\alpha}(t) = I_R^{S\alpha}(t)$, for the case of an insulating ferromagnetic wire generated by using $\gamma_{ij} = 0$ for the hopping between tight-binding sites in Eq. (2) within the active region. The Fermi energy is chosen as $E_F = -1.6$ eV and dc bias voltage is absent, $V_b = 0$.

around an easy axis with frequency ω and precession cone angle θ , as illustrated in Fig. 1. The cone angle has even been measured [8] as $\theta \lesssim 10^\circ$.

In this Rapid Communication, we employ recently developed multiscale time-dependent-quantum-transport/classical-micromagnetics formalism [40–42] to the problem of electron-SW interaction which makes possible treating large number of localized spins in experimentally relevant noncollinear configurations and over time scales reaching ~ 1 ns. The formalism combines time-dependent nonequilibrium Green functions (TD-NEGF) [36, 43] description of electrons out of equilibrium in open systems, such as those illustrated in Fig. 1, with the Landau-Lifshitz-Gilbert (LLG) equation describing classical dynamics of localized magnetic moments. The classical treatment of localized magnetic moments is justified [44] in the limit of large localized spins $S \rightarrow \infty$ and $\hbar \rightarrow 0$ (while $S \times \hbar \rightarrow 1$), as well as in the absence of entanglement between quantum state of localized spins (which otherwise causes change in their expectation value due to decoherence [45]) as expected to be satisfied at room temperature.

In fact, since we assume that a single coherent SW has been excited externally, such as by microwave current flowing through narrow antennas [9], we fix dynamics of localized magnetic moment $\mathbf{M}_i(t)$ at site i of a one-dimensional (1D) lattice to be the SW solution [4] of the

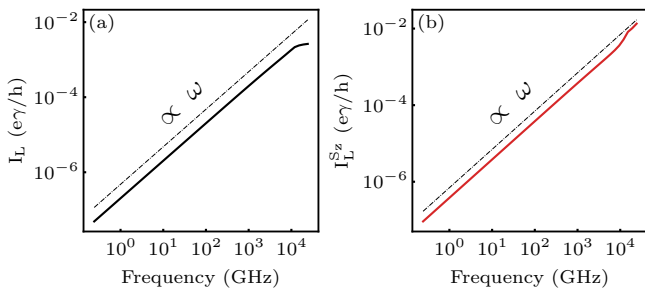


FIG. 4. Frequency-dependence of electronic (a) charge I_L and (b) spin $I_L^{S_z}$ currents in the left NM lead which are time independent as shown in Fig. 3(c) and Fig. 3(a), respectively. The dash-dot lines demonstrate that these dependences are linear $\propto \omega$ in the GHz–THz frequency range for magnetization dynamics of realistic materials [5].

LLG equation (for simplicity without damping):

$$\mathbf{M}_i^x(t) = \sin \theta \cos(kx_i + \omega t), \quad (1a)$$

$$\mathbf{M}_i^y(t) = \sin \theta \sin(kx_i + \omega t), \quad (1b)$$

$$\mathbf{M}_i^z(t) = \cos \theta. \quad (1c)$$

Due to 1D geometry, the wavevector is just a number $k = 2\pi/[a(N-1)] = 2\pi/\lambda$, while the discrete coordinate is $x_i = (i-1)a$ and $N = 10$ is chosen as the total number of localized magnetic moments. Note that the *uniform mode*—which describes all magnetic moments precessing in-phase in magnetic materials driven by microwaves under the ferromagnetic resonance conditions [46]—is obtained simply by setting $k = 0$. Although 1D geometry is chosen for simplicity, and it appears at first sight like a toy model of a realistic three-dimensional FM layer, it has been actually realized experimentally as an artificial chain of (up to six) ferromagnetically coupled Fe atoms whose SWs were excited and detected using atom-resolved inelastic tunneling spectroscopy in a scanning tunneling microscope [7].

The FM nanowire hosting such SW is an active region of devices in Fig. 1, which is attached to two normal metal (NM) semi-infinite leads terminating into the macroscopic reservoirs. We use three different two-terminal geometries depicted Fig. 1: (a) no bias voltage V_b is applied between the left (L) and right (R) reservoirs kept at the same chemical potential $\mu_L = \mu_R$; (b) small dc bias voltage, $eV_b = \mu_L - \mu_R = 0.01$ eV, is applied between the reservoirs to inject unpolarized charge current into the active region where electrons are spin-polarized by three static localized magnetic moments [red arrows in Fig. 1(b)] pointing along the z -axis; and (c) the Lorentzian voltage pulse [22, 23] applied to the left NM lead injects a “leviton” current pulse $I_L(t)$ carrying charge $\int dt I_L(t) = 2e$, which is then spin-polarized by the same three static localized magnetic moments as in (b).

The quantum Hamiltonian of electrons within the FM

nanowire is chosen as 1D tight-binding model

$$\hat{H}(t) = - \sum_{\langle ij \rangle} \gamma_{ij} \hat{c}_i^\dagger \hat{c}_j - J_{sd} \sum_i \hat{c}_i^\dagger \boldsymbol{\sigma} \cdot \mathbf{M}_i(t) \hat{c}_i, \quad (2)$$

with an additional sd exchange interaction of strength $J_{sd} = 0.5$ eV between the spins of the conduction electrons, described by the vector of the Pauli matrices $\boldsymbol{\sigma} = (\hat{\sigma}_x, \hat{\sigma}_y, \hat{\sigma}_z)$, and $\mathbf{M}_i(t)$ from Eq. (1). Here $\hat{c}_i^\dagger = (\hat{c}_{i\uparrow}^\dagger, \hat{c}_{i\downarrow}^\dagger)$ is a row vector containing operators $\hat{c}_{i\sigma}^\dagger$ which create an electron with spin $\sigma = \uparrow, \downarrow$ at site i ; \hat{c}_i is a column vector containing the corresponding annihilation operators; and $\gamma_{ij} = 1$ eV is the nearest-neighbor hopping. The NM leads are described by the same Hamiltonian as Eq. (2) but with $J_{sd} \equiv 0$.

The fundamental quantity of nonequilibrium quantum statistical mechanics is the density matrix. The time-dependent one-particle density matrix can be expressed [43], $\boldsymbol{\rho}_{\text{neq}}(t) = \mathbf{G}^<(t, t)/i$, in terms of the lesser Green function of TDNEGF formalism defined by $G_{ii'}^<,\sigma\sigma'(t, t') = i\langle \hat{c}_{i'\sigma'}^\dagger(t') \hat{c}_{i\sigma}(t) \rangle$ where $\langle \dots \rangle$ is the nonequilibrium statistical average [36]. We solve a matrix integro-differential equation [47]

$$i\hbar \frac{d\boldsymbol{\rho}_{\text{neq}}}{dt} = [\mathbf{H}(t), \boldsymbol{\rho}_{\text{neq}}] + i \sum_{p=L,R} [\boldsymbol{\Pi}_p(t) + \boldsymbol{\Pi}_p^\dagger(t)], \quad (3)$$

for the time evolution of $\boldsymbol{\rho}_{\text{neq}}(t)$ where $\mathbf{H}(t)$ is the matrix representation of Hamiltonian in Eq. (2). This can be viewed as an exact master equation for an open finite-size quantum system attached to macroscopic Fermi liquid reservoirs via semi-infinite NM leads that ensure continuous energy spectrum of the system. The $\boldsymbol{\Pi}_p(t)$ matrices

$$\boldsymbol{\Pi}_p(t) = \int_{t_0}^t dt_2 [\mathbf{G}^>(t, t_2) \boldsymbol{\Sigma}_p^<(t_2, t) - \mathbf{G}^<(t, t_2) \boldsymbol{\Sigma}_p^>(t_2, t)], \quad (4)$$

are expressed in terms of the lesser and greater Green function and the corresponding self-energies $\boldsymbol{\Sigma}_p^>,\<(t, t')$ [47]. They yield directly time-dependent total charge, $I_p(t) = \frac{e}{\hbar} \text{Tr} [\boldsymbol{\Pi}_p(t)]$, and spin, $I_p^{S_\alpha}(t) = \frac{e}{\hbar} \text{Tr} [\hat{\sigma}_\alpha \boldsymbol{\Pi}_p(t)]$, currents flowing into the lead $p = L, R$. Local currents [48], or any other local quantity within the active region, are obtained by tracing the corresponding operator with $\boldsymbol{\rho}_{\text{neq}}(t)$. We use the same units for charge and spin currents, defined as $I_p = I_p^\uparrow + I_p^\downarrow$ and $I_p^{S_\alpha} = I_p^\uparrow - I_p^\downarrow$, in terms of spin-resolved charge currents I_p^σ . In our convention, *positive* current in NM lead p means charge or spin is flowing *out* of that lead.

We build intuition step-by-step by first confirming standard spin pumping by the uniform mode [46, 49–51], with $k = 0$ in Eq. (1) and no dc bias voltage applied, which then serves as a reference point for subsequent discussion. In this case, identical *pure* (i.e., not accompanied by any charge current) spin currents $I_L^{S_\alpha}(t) = I_R^{S_\alpha}(t)$ are pumped into both leads, as shown in Fig. 2. Their $I_L^{S_z} = I_R^{S_z}$ components are time independent, and their negative sign shows that they flow *into* the NM leads, as

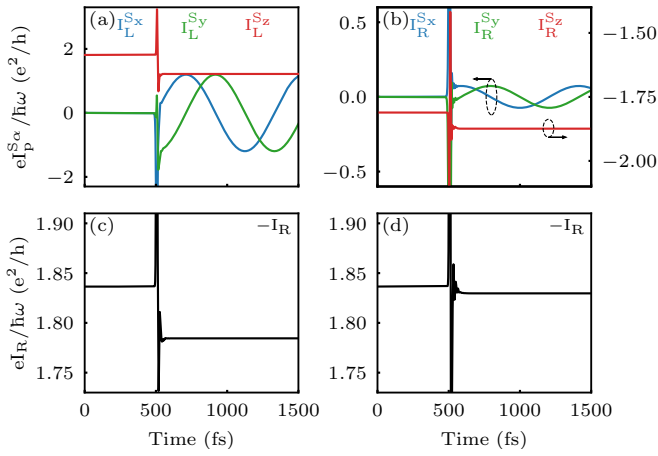


FIG. 5. Time-dependence of electronic spin currents in the (a) left and (b) right NM leads of setup in Fig. 1(b) whose localized magnetic moments start to precess at $t = 500$ fs as a coherent SW with $k \neq 0$ in Eq. (1) in the presence of a flux of electrons injected into the active region by the external dc bias voltage $eV_b = 0.01$ eV. The injected electrons become spin-polarized due to three fixed spins (red arrows) in Fig. 1(b). The corresponding time-dependence of their charge current $I_R(t)$ is shown in panel (c). Panel (d) plots time dependence of $I_R(t)$ for “frozen-in-time” [25] SW where $t = 0$ in Eq. (1). The Fermi energy is chosen as $E_F = -1.6$ eV and dc bias voltage is $V_b = 0.01$ V.

obtained also in the scattering theory [46], rotating frame approach [49] or Floquet-NEGF theory [50, 51].

On the other hand, the excited SW in the setup of Fig. 1(a) pumps *both* spin and charge currents into the NM leads in the absence of any dc bias voltage. Their time dependences, $I_p^{S\alpha}(t)$ and $I_p(t)$, are shown in Fig. 2 after transient currents have died out. Furthermore, in contrast to pumping by the uniform mode, $|I_L^{S_z}| > |I_R^{S_z}|$, which is due to spin current carried by the SW itself [12]. That is, spin current carried by the SW must be “transmuted” into electronic spin current at the FM-wire/NM-left-lead interface [10, 12, 42] since no localized magnetic moments exists in the NM lead to support transport of angular momentum via their dynamics. This currents is then added or subtracted to symmetrically pumped spin currents into the left or right NM leads, respectively. This interpretation is supported by the fact that changing the sign of k in Eq. (1) leads to a reversed situation, $|I_L^{S_z}| < |I_R^{S_z}|$.

The charge pumping in spintronic devices with excited coherent SWs has been observed recently in the experiments on compressively strained (Ga,Mn)As bar [52] or YIG/graphene [9] heterostructures (where SWs are excited within YIG). However, both of these setups require the presence of SO coupling. In fact, SO coupling present directly at the interface of FM/NM heterostructures leads to pumping of charge current even for uniform mode of magnetization precession within the FM layer [28]. Thus, the charge pumping by SW in the ab-

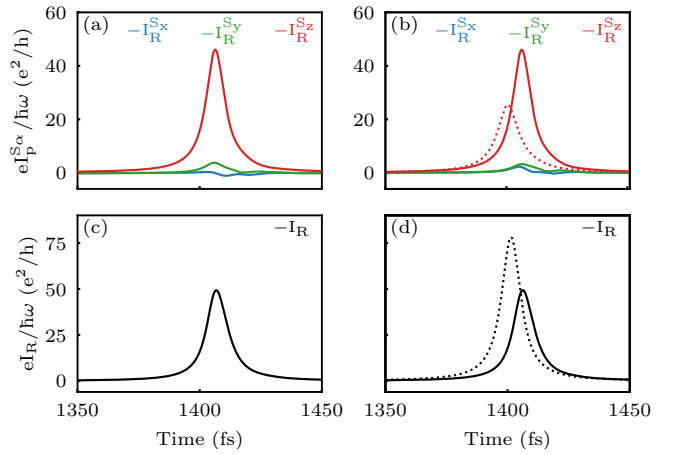


FIG. 6. Time-dependence of electronic spin currents $I_R^{S\alpha}(t)$ in the right NM lead after unpolarized “leviton” is injected by the Lorentzian voltage pulse [22, 23] into the active region hosting: (a) three static localized magnetic moments (red arrows) along the z -axis, acting as spin-polarizer, followed by SW excited at $t = 500$ fs, as illustrated in Fig. 1(c); (b) three static localized magnetic moments and a “frozen-in-time” SW excited at $t = 500$ fs. Panels (c) and (d) show time dependence of the charge current $I_R(t)$ corresponding to (a) and (b), respectively. In addition, panels (b) and (d) plot (dotted lines) time dependence of $I_R^{S\alpha}(t)$ and $I_R(t)$, respectively, for the active region containing only the three static localized magnetic moments. The Fermi energy is chosen as $E_F = -1.6$ eV. The solid lines in panels (a)–(d) are also animated as two movies provided in the SM [57].

sence of any SO coupling predicted by Fig. 3(c) appears to be a novel effect which calls for physical interpretation of its origin.

To assist such interpretation, we compute frequency dependence of pumped charge current I_L [Fig. 4(a)], as well as of spin current $I_L^{S_z}$ [Fig. 4(b)]. Both scale linearly in the physically relevant frequency range GHz–THz [5]. This is in contrast to, e.g., charge pumping by SW in YIG/graphene heterostructure where sizable effect is observed between 5 and 7 GHz only [9]. We recall that such linear scaling is in accord with the key requirement—*breaking of left-right symmetry*—for nonzero dc component of quantum charge pumping by a time-dependent potential [48, 53, 54]. This can be achieved by breaking inversion symmetry and/or time-reversal symmetry. In the adiabatic regime, quantum charge pumping requires both inversion and time-reversal symmetries to be broken dynamically, such as by two spatially separated potentials oscillating out-of-phase [53], which leads to $\bar{I}_p(t) \propto \omega$ (where \bar{A} is average over one period) at low frequencies. In the case of SW, it is the wave-like pattern of precessing localized magnetic moments which dynamically breaks the left-right symmetry in Fig. 1(a), with respect to vertical plane positioned between moments localized at sites $i = 5$ and $i = 6$. In contrast, in the nonadiabatic regime only one of those two symmetries needs to be broken and this does not have to occur dy-

namicly. The DC component of the pumped current in the nonadiabatic regime is [54] $\bar{I}_p(t) \propto \omega^2$ at low frequencies as obtained in, e.g., the case of charge pumping by uniform mode across potential barrier that breaks the left-right symmetry of the device statically [49].

In Fig. 3(d) we also examine pumping from NM-lead/ferromagnetic-insulator/NM-lead setup, which is the same geometry as in Fig. 1(a) but with $\gamma_{ij} = 0$ within the active region and $\gamma_{ij} \neq 0$ in the NM leads or between the leads and the active region. In this case, only the two localized magnetic moments at the edges (i.e., those at sites $i = 1$ and $i = 10$) are coupled to conduction electrons and are pumping pure spin current in Fig. 3(d), of similar magnitude as the uniform mode in Fig. 2, while pumping of charge current is absent. Thus, this clarifies that charge and spin pumping driven by SW are obtained through interference of currents pumped by all localized magnetic moments, in the bulk and at the interface.

For the setup in Fig. 1(b), we first establish (after some transient period not shown explicitly) steady charge current I_R [flat line in Fig. 5(c) for $t < 500$ fs] of electrons injected by dc bias voltage into 3 + 10 static localized magnetic moments oriented along the z -axis. This current also becomes spin-polarized due to their presence, as characterized by steady spin current $I_R^{S_z} \neq 0$ [flat line in Fig. 5(b) for $t < 500$ fs] and the corresponding spin-polarization $P_z = |I_R^{S_z}|/|I_R| \approx 50\%$. Then at $t = 500$ fs we *suddenly* excite SW composed of 10 precessing localized magnetic moments in Fig. 1(b), leading to transient currents at that instant that help us to visualize the boundary between the time interval without and with SW being present. Within the time interval $t > 500$ fs where SW is present, new time-dependent spin currents $I_p^{S_x}(t)$ and $I_p^{S_y}(t)$ emerge [Fig. 5(a),(b)] due to spin pumping by SW demonstrated in Fig. 3.

Concurrently, dc spin currents $I_L^{S_z}$ [Fig. 5(a)] and $I_R^{S_z}$ [Fig. 5(b)], as well as dc charge current I_R [Fig. 5(c)], are reduced compared to their values prior to SW excitation. This reduction is mostly due to charge and spin currents pumped in the direction right-NM-lead \rightarrow left-NM-lead in Fig. 3, which is opposite to the flow of originally injected charge and spin currents by dc bias voltage. Thus, outflowing spin and charge currents in the right NM lead can also be enhanced if we invert the sign of k in Eq. (1) and, therefore, the direction of SW propagation. Another reason for the reduction is backscattering of electrons by time-dependent potential generated by SW, whose magnitude for charge current shown in Fig. 5(c) we estimate using $[I_R(t < 500 \text{ fs}) - I_R(t > 500 \text{ fs}) + I_R^{\text{SW}}]/I_R(t < 500 \text{ fs})$ to be less than 1%. Here I_R^{SW} denotes charge current pumped by SW in Fig. 3(c).

Recent time-independent quantum transport calculations [25] of the resistance of FM have include “frozen magnons” as correlated spin disorder where localized

spins are tilted away from the easy axis in accord with thermal population of magnon modes. To understand time-dependent effects missed in such calculations, we freeze localized magnetic moments by setting $t = 0$ in Eq. (1). The scattering from such “frozen-in-time” SW leads to much smaller current reduction in Fig. 5(d).

Finally, in order to simulate single-electron–single-SW scattering, we inject pulsed current into the active region using the Lorentzian voltage pulse [47], $V_L(t) = 2\hbar\tau/[(t - t_0)^2 - \tau^2]$, where the pulse duration is $\tau = 7.5\hbar/\gamma$. As confirmed experimentally [55], such special profile with $\frac{e}{\hbar} \int dt V_L(t) = 2\pi n$ [56] driving the Fermi sea in the left reservoir ensures [22, 23] excitation of an integer number n of purely electronic states above the sea, without spurious electron-hole pairs and with minimal nonequilibrium noise in transfer across the active region. We use $n = 2$, so that injected unpolarized charge current pulse called “leviton” carries charge $\int dt I_L(t) = 2e$. This can be viewed as minimalistic unpolarized current composed of one spin- \uparrow and one spin- \downarrow electron flowing together. Upon spin-polarization by three static localized magnetic moments in Fig. 1(c), the “leviton” interacts with SW excited suddenly at $t = 500$ fs. After such interaction, “leviton” outflows into the right NM lead where its spin and charge currents are given in Figs. 6(a) and 6(c), respectively. For comparison, Figs. 6(b) and 6(d) plot spin and charge currents in the right NM lead, respectively, for a “leviton” interacting with “frozen-in-time” SW. Solid lines in Fig. 6 for both cases are animated as two movies in the Supplemental Material [57]. In addition, Figs. 6(b) and 6(d) also include (dotted lines) spin and charge current of “leviton” outflowing into the right NM lead when SW in Fig. 1(c) is removed from the active region. The integrals for outflowing spin-polarized “leviton” after scattering from SW in Figs. 6(a) and 6(c) are $\int dt I_R^{S_z}(t) = 0.939e$ and $\int dt I_R(t) = 0.822e$, respectively. They can be compared to $\int dt I_R^{S_z}(t) = 0.944e$ and $\int dt I_R(t) = 0.827e$ in Figs. 6(b) and 6(d), respectively. Note that the ratio of integrals of two dotted curves in Figs. 6(b) and 6(d) is $P_z = |\int dt I_R^{S_z}(t)|/|\int dt I_R(t)| \approx 40\%$ which can be considered as the spin-polarization of “leviton” after passing through three static localized magnetic moments in Fig. 1(c).

ACKNOWLEDGMENTS

This research was supported in part by the US National Science Foundation under Grant No. ECCS-1922689. It was finalized during “Spin and Heat Transport in Quantum and Topological Materials” program at KITP Santa Barbara, which is supported under Grant No. PHY-1748958.

- [1] C. Friedrich, M. C. T. D. Müller, and S. Blügel, Spin excitations in solid from many-body perturbation theory, in W. Andreoni and S. Yip (eds.) *Handbook of Materials Modeling* (Springer, Cham, 2019).
- [2] M. C. T. D. Müller, S. Blügel, and C. Friedrich, Electron-magnon scattering in elementary ferromagnets from first principles: Lifetime broadening and band anomalies, *Phys. Rev. B* **100**, 045130 (2019).
- [3] E. Młyńczak *et al.*, Kink far below the Fermi level reveals new electron-magnon scattering channel in Fe, *Nat. Commun.* **10**, 505 (2019).
- [4] S.-K. Kim, Micromagnetic computer simulations of spin waves in nanometre-scale patterned magnetic elements, *J. Phys. D: Appl. Phys.* **43**, 264004 (2010).
- [5] B. Jungfleisch, W. Zhang, and A. Hoffmann, Perspectives of antiferromagnetic spintronics, *Phys. Lett. A* **382**, 865 (2018).
- [6] P. E. Zil'berman, A. G. Terniryazev, and M. P. Tikhornirova, Excitation and propagation of exchange spin waves in films of yttrium iron garnet, *JETP* **81**, 151 (1995).
- [7] A. Spinelli, B. Bryant, F. Delgado, J. Fernández-Rossier, and A. F. Otte, Imaging of spin waves in atomically designed nanomagnets, *Nat. Mater.* **10**, 782 (2014).
- [8] V. E. Demidov, U.-H. Hansen, and S. O. Demokritov, Spin-wave eigenmodes of a saturated magnetic square at different precession angles, *Phys. Rev. Lett.* **98**, 157203 (2007).
- [9] M. Evelt, H. Ochoa, O. Dzyapko, V. E. Demidov, A. Yurgens, J. Sun, Y. Tserkovnyak, V. Bessonov, A. B. Rinkevich, and S. O. Demokritov, Chiral charge pumping in graphene deposited on a magnetic insulator, *Phys. Rev. B* **95**, 024408 (2017).
- [10] S. Woo, T. Delaney, and G. S. D. Beach, Magnetic domain wall depinning assisted by spin wave bursts, *Nat. Phys.* **13**, 448 (2017).
- [11] C. Tzschaschel, K. Otani, R. Iida, T. Shimura, H. Ueda, S. Günther, M. Fiebig, and T. Satoh, Ultrafast optical excitation of coherent magnons in antiferromagnetic NiO, *Phys. Rev. B* **95**, 174407 (2017).
- [12] C. W. Sandweg, Y. Kajiwara, A. V. Chumak, A. A. Serga, V. I. Vasyuchka, M. B. Jungfleisch, E. Saitoh, and B. Hillebrands, Spin pumping by parametrically excited exchange magnons, *Phys. Rev. Lett.* **106**, 216601 (2011).
- [13] M. Kargarian, D. K. Efimkin, and V. Galitski, Amperean pairing at the surface of topological insulators, *Phys. Rev. Lett.* **117**, 076806 (2016).
- [14] N. Rohling, E. L. Fjærby, and A. Brataas, Superconductivity induced by interfacial coupling to magnons, *Phys. Rev. B* **97**, 115401 (2018).
- [15] L. Bulaevskii, R. Eneias, and A. Ferraz, Triplet superconductivity in ferromagnets due to magnon exchange, *Phys. Rev. B* **99**, 064506 (2019).
- [16] M. M. Müller, C. P. J. Adolphs, and M. Berciu, Magnon-mediated attraction between two holes doped in a CuO₂ layer, *Phys. Rev. B* **100**, 165118 (2019).
- [17] P. Richmond, An electron in a ferromagnetic crystal (the magnetic polaron), *J. Phys. C* **3**, 2402 (1970).
- [18] B. Sriram Shastry and D. C. Mattis, Theory of the magnetic polaron, *Phys. Rev. B* **24**, 5340 (1981).
- [19] D. I. Marvakov, A. L. Kuzemsky, and J. P. Vlahov, A self-consistent theory of the magnetic polaron, *Physica* **138B**, 129 (1986).
- [20] F. Reininghaus, T. Korb, and H. Schoeller, Fingerprints of the magnetic polaron in nonequilibrium electron transport through a quantum wire coupled to a ferromagnetic spin chain, *Phys. Rev. Lett.* **97**, 026803 (2006).
- [21] M. Moëller, G. A. Sawatzky, and M. Berciu, Magnon-mediated interactions between fermions depend strongly on the lattice structure, *Phys. Rev. Lett.* **108**, 216403 (2012).
- [22] D. Ivanov, H. Lee, and L. Levitov, Coherent states of alternating current, *Phys. Rev. B* **56**, 6839 (1997).
- [23] J. Keeling, I. Klich, and L. Levitov, Minimal excitation states of electrons in one-dimensional wires, *Phys. Rev. Lett.* **97**, 116403 (2006).
- [24] B. Raquet, M. Viret, E. Sondergard, O. Cespedes, and R. Mamy, Electron-magnon scattering and magnetic resistivity in 3d ferromagnets, *Phys. Rev. B* **66**, 024433 (2002).
- [25] A. A. Starikov, Y. Liu, Z. Yuan, and P. J. Kelly, Calculating the transport properties of magnetic materials from first principles including thermal and alloy disorder, noncollinearity, and spin-orbit coupling, *Phys. Rev. B* **97**, 214415 (2018).
- [26] E. Carpena, E. Mancini, C. Dallera, M. Brenna, E. Puppin, and S. De Silvestri, Dynamics of electron-magnon interaction and ultrafast demagnetization in thin iron films, *Phys. Rev. B* **78**, 174422 (2008).
- [27] V. Drewello, J. Schmalhorst, A. Thomas, and G. Reiss, Evidence for strong magnon contribution to the TMR temperature dependence in MgO based tunnel junctions, *Phys. Rev. B* **77**, 014440 (2008).
- [28] F. Mahfouzi and B. K. Nikolić, Signatures of electron-magnon interaction in charge and spin currents through magnetic tunnel junctions: A nonequilibrium many-body perturbation theory approach, *Phys. Rev. B* **90**, 045115 (2014).
- [29] J. C. Slonczewski and J. Z. Sun, Theory of voltage-driven current and torque in magnetic tunnel junctions, *J. Magn. Magn. Mater.* **310**, 169 (2007).
- [30] T. Balashov, A. F. Takács, M. Däne, A. Ernst, P. Bruno, and W. Wulfhekel, *Phys. Rev. B* **78**, 174404 (2008).
- [31] Y. Cheng, W. Wang, and S. Zhang, Amplification of spin-transfer torque in magnetic tunnel junctions with an antiferromagnetic barrier, *Phys. Rev. B* **99**, 104417 (2019).
- [32] N. Okuma and K. Nomura, Microscopic derivation of magnon spin current in a topological insulator/ferromagnet heterostructure, *Phys. Rev. B* **95**, 115403 (2017).
- [33] Y. Kajiwara, K. Harii, S. Takahashi, J. Ohe, K. Uchida, M. Mizuguchi, H. Umezawa, H. Kawai, K. Ando, K. Takanashi, S. Maekawa and E. Saitoh, Transmission of electrical signals by spin-wave interconversion in a magnetic insulator, *Nature* **464**, 262 (2010).
- [34] J. Zheng, S. Bender, J. Armaitis, R. E. Troncoso, and R. A. Duine, Green's function formalism for spin transport in metal-insulator-metal heterostructures, *Phys. Rev. B* **96**, 174422 (2017).
- [35] K. Uchida, J. Xiao, H. Adachi, J. Ohe, S. Takahashi, J. Ieda, T. Ota, Y. Kajiwara, H. Umezawa, H. Kawai, G. E. W. Bauer, S. Maekawa and E. Saitoh, Spin Seebeck

- insulator, *Nat. Mater.* **9**, 894 (2010).
- [36] G. Stefanucci and R. van Leeuwen, *Nonequilibrium Many-Body Theory of Quantum Systems: A Modern Introduction* (Cambridge University Press, Cambridge, 2013).
- [37] M. N. Kiselev and R. Oppermann, Schwinger-Keldysh semionic approach for quantum spin systems, *Phys. Rev. Lett.* **85**, 5631 (2000).
- [38] H. Mera, T. G. Pedersen, B. K. Nikolić, Hypergeometric resummation of self-consistent sunset diagrams for steady-state electron-boson quantum many-body systems out of equilibrium, *Phys. Rev. B* **94**, 165429 (2016).
- [39] J. Gukelberger, L. Huang, and P. Werner, On the dangers of partial diagrammatic summations: Benchmarks for the two-dimensional Hubbard model in the weak-coupling regime, *Phys. Rev. B* **91**, 235114 (2015).
- [40] M. D. Petrović, B. S. Popescu, U. Bajpai, P. Plecháč, and B. K. Nikolić, Spin and charge pumping by a steady or pulse-current-driven magnetic domain wall: A self-consistent multiscale time-dependent quantum-classical hybrid approach, *Phys. Rev. Applied* **10**, 054038 (2018).
- [41] U. Bajpai and B. K. Nikolić, Time-retarded damping and magnetic inertia in the Landau-Lifshitz-Gilbert equation self-consistently coupled to electronic time-dependent nonequilibrium Green functions, *Phys. Rev. B* **99**, 134409 (2019).
- [42] M. D. Petrović, P. Plecháč, and B. K. Nikolić, Annihilation of topological solitons in magnetism: How domain walls collide and vanish to burst spin waves and pump electronic spin current of broadband frequencies, [arXiv:1905.01299](https://arxiv.org/abs/1905.01299) (2019).
- [43] B. Gaury, J. Weston, M. Santin, M. Houzet, C. Groth, and X. Waintal, Numerical simulations of time-resolved quantum electronics, *Phys. Rep.* **534**, 1 (2014).
- [44] R. Wieser, Description of a dissipative quantum spin dynamics with a Landau-Lifshitz-Gilbert like damping and complete derivation of the classical Landau-Lifshitz equation, *Euro. Phys. J. B* **88**, 77 (2015).
- [45] P. Mondal, U. Bajpai, M. D. Petrović, P. P. Plecháč, and B. K. Nikolić, Quantum spin-transfer torque induced nonclassical magnetization dynamics and electron-magnetization entanglement, *Phys. Rev. B* **99**, 094431 (2019).
- [46] Y. Tserkovnyak, A. Brataas, G. E. W. Bauer, and B. I. Halperin, Nonlocal magnetization dynamics in ferromagnetic heterostructures, *Rev. Mod. Phys.* **77**, 1375 (2005).
- [47] B. Popescu and A. Croy, Efficient auxiliary-mode approach for time-dependent nanoelectronics, *New J. Phys.* **18**, 093044 (2016).
- [48] U. Bajpai, B. S. Popescu, P. Plecháč, B. K. Nikolić, L. E. F. Foa Torres, H. Ishizuka, and N. Nagaosa, Spatio-temporal dynamics of shift current quantum pumping by femtosecond light pulse, *J. Phys.: Mater.* **2**, 025004 (2019).
- [49] S.-H. Chen, C.-R. Chang, J. Q. Xiao, and B. K. Nikolić, *Phys. Rev. B* **79**, 054424 (2009).
- [50] F. Mahfouzi, J. Fabian, N. Nagaosa, and B. K. Nikolić, Charge pumping by magnetization dynamics in magnetic and semimagnetic tunnel junctions with interfacial Rashba or bulk extrinsic spin-orbit coupling, *Phys. Rev. B* **85**, 054406 (2012).
- [51] K. Dolui, U. Bajpai, and B. K. Nikolić, Effective spin-mixing conductance of topological-insulator/ferromagnet and heavy-metal/ferromagnet spin-orbit-coupled interfaces: A first-principles Floquet-nonequilibrium-Green-function approach, [arXiv:1905.01299](https://arxiv.org/abs/1905.01299) (2019).
- [52] C. Ciccarelli, K. M. D. Hals, A. Irvine, V. Novak, Y. Tserkovnyak, H. Kurebayashi, A. Brataas, and A. Ferguson, Magnonic charge pumping via spin-orbit coupling, *Nat. Nanotechnol.* **10**, 50 (2014).
- [53] M. Moskalets and M. Büttiker, Floquet scattering theory of quantum pump, *Phys. Rev. B* **66**, 205320 (2002).
- [54] L. E. F. Foa Torres, Mono-parametric quantum charge pumping: Interplay between spatial interference and photon-assisted tunneling, *Phys. Rev. B* **72**, 245339 (2005).
- [55] J. Dubois, T. Jullien, F. Portier, P. Roche, A. Cavanna, Y. Jin, W. Wegscheider, P. Roulleau, and D. Glattli, Minimal-excitation states for electron quantum optics using levitons, *Nature* **502**, 659 (2013).
- [56] M. Moskalets, Fractionally charged zero-energy single-particle excitations in a driven Fermi sea, *Phys. Rev. Lett.* **117**, 046801 (2016).
- [57] See Supplemental Material at <https://wiki.physics.udel.edu/qttg/Publications> for two movies accompanying Fig. 6, which animate time evolution of spin-polarized leviton in the course of its scattering from SW [Fig. 6(a),(c)] or “frozen-in-time” SW [Fig. 6(b),(d)].